Differential Susceptibility of Escherichia coli Cells toward Transition Metal-Doped and Matrix-Embedded ZnO Nanoparticles

ARTICLE *in* THE JOURNAL OF PHYSICAL CHEMISTRY B · APRIL 2010

Impact Factor: 3.3 · DOI: 10.1021/jp1004488 · Source: PubMed

5 AUTHORS, INCLUDING:

Prashant K. Sharma
Indian School of Mines
112 PUBLICATIONS **1,058** CITATIONS
SEE PROFILE

Richa Bhargava
Motilal Nehru National Institute of Technol…
17 PUBLICATIONS **154** CITATIONS
SEE PROFILE

Naresh Kumar
Motilal Nehru National Institute of Technol…
36 PUBLICATIONS **303** CITATIONS
SEE PROFILE

Avinash C Pandey
Professor, University of Allahabad
267 PUBLICATIONS **2,097** CITATIONS
SEE PROFILE

Differential Susceptibility of *Escherichia coli* Cells toward Transition Metal-Doped and Matrix-Embedded ZnO Nanoparticles

Ranu K. Dutta,*,† Prashant K. Sharma,† Richa Bhargava,‡ Naresh Kumar,‡ and Avinash C. Pandey†

Nanotechnology Application Centre, University of Allahabad, Allahabad 211002, India, Department of Physics, Motilal Nehru National Institute of Technology, Allahabad 211004, India

Received: January 17, 2010; Revised Manuscript Received: February 21, 2010

Dependence of the antibacterial behavior on ZnO (TM-doped and surface-modified) nanoparticles on *Escherichia coli* cells has been investigated. ZnO nanoparticles that differ in size, activator ion and in the microenvironment in which these nanoparticles are embedded were used. Comprehensive antibacterial studies of these ZnO nanoparticles owing to their size and surface defects are carried out against *E. coli* cells. These studies have been carried out both in Luria−Bertani medium and on solid agar medium in the presence and absence of light. The differences in antibacterial effect have been quantified in terms of minimum inhibitory concentration, minimum bactericidal concentration, colony forming unit counts, and qualitatively evaluated by growth curves and disk diffusion tests. The difference in antibacterial activities of the ZnO nanoparticles may be attributed to the enhanced or reduced oxygen vacancies and defect states and could be attributed to the increased or decreased surface defects.

1. Introduction

ZnO, a wide-band-gap semiconductor and piezoelectric material with energy band gap of 3.3 eV,[1] has been used for a variety of applications. Nanoscale (20−100 nm) ZnO has been employed as a safe, physical sunscreen because it scatters and reflects ultraviolet (UV) radiation in sunlight. ZnO nanoparticles are believed to be nontoxic, biosafe, and biocompatible[2] and have also been used as drug carriers and in cosmetics and fillings in medical materials.[3,4] Physical parameters such as surface area, particle size, surface charge, and ζ potential are very important for providing mechanistic details in the uptake, persistence, and biological toxicity of nanoparticles inside living cells. Several reports have highlighted the harmful impact of nanomaterials on living cells. Although many studies on the biological activity of ZnO have been carried out, most of these pertain to the antimicrobial effect of bulk ZnO with a large particle size. Yamamoto et al.[5] studied the antibacterial activity of ZnO having particle sizes in the range of 100 nm−1 μm. Reddy et al.[6] studied the effects of ZnO on both prokaryotic and eukaryotic cells, and the comparative ecotoxicity of nanoscale TiO_2, SiO_2, and ZnO water suspensions were studied by Adams et al.[7] Wang et al.[8] proposed that the orientation of ZnO can also affect bioactivity. Gedanken et al.[9] proposed that the main mechanism behind toxicity is the formation of reactive oxygen species (ROS). The effects of the lattice constant of ZnO on antibacterial properties have been also studied by Yamamoto et al.[10] Electron spin resonance measurements revealed that aqueous suspensions of small nanoparticles of ZnO produce increased levels of reactive oxygen species; namely, hydroxyl radicals and singlet oxygen.[11] Interestingly, a remarkable enhancement of the oxy radicals was detected when a ZnO water suspension had been irradiated with blue (400−500 nm) light.

Most of these studies pertain to toxic effects of ZnO only. No such work has been done toward investigation of the antibacterial properties of transition metal (TM)-doped ZnO and how the defect-related properties influence the antibacterial properties. The increased production of nanoparticles (NPs) is making it more likely that such materials will end up in watercourses as either medical or industrial waste or, when used as ecological tools, with unknown consequences for microbial and aquatic life. Since almost all dilute magnetic semiconductor (DMS)-based applications are based on transition-metal-doped ZnO, therefore, it is important to investigate the effects of doped ZnO nanoparticles on living systems. In the same pursuit, we have investigated the antibacterial activity of some ZnO nanoparticles; namely, commercial ZnO (∼200−300 nm); ZnO (∼25 nm); Fe^{2+}- and Co^{2+}-doped ZnO (∼25−30 nm); and ZnO@SiO_2 (∼25 nm size), in which ZnO has been embedded in a SiO_2 matrix against *Escherichia coli* (DH 5α) as the model organism.

The objectives of the present study were to find out (a) what role the change in oxygen vacancies plays in governing the antibacterial properties of ZnO; (b) the effects of size, dopant, and modifications in the host ZnO on the antibacterial properties; (c) the concentrations at which the ZnO nanoparticle suspensions are toxic to bacterial cells; and (d) the effect of light on the variance in toxicity of the nanoparticles toward bacteria. Attempts have been made to establish a correlation between the functional properties of these particles and the associated antibacterial mechanism. These nanoparticles were synthesized and characterized thoroughly by X-ray diffraction (XRD), transmission electrom microscopy (TEM) and micro-Raman spectroscopy. The comprehensive antibacterial studies have been carried out both in Luria−Bertani medium and on solid agar medium in the presence and absence of light. The differences in the antibacterial effect have been quantified in terms of minimum inhibitory concentration (MIC), minimum bactericidal

* Corresponding author. Phone/Fax: +91-532-2460675. E-mail: ranu.dutta16@gmail.com.
† University of Allahabad.
‡ Motilal Nehru National Institute of Technology.

10.1021/jp1004488
Published on Web 04/06/2010

concentration (MBC), and colony forming unit (CFU) counts and qualitatively evaluated by growth curves and disk diffusion tests.

2. Materials and Methods

2.1. Synthesis of ZnO Nanoparticles. We used commercial bulk ZnO (200−300 nm in size, 99.99% pure), procured from E. Merck Ltd., India. For synthesis of ZnO nanoparticles, analytical reagent grade zinc acetate dihydrate (99.2%) $Zn(CH_3COO)_2 \cdot 2H_2O$, potassium hydroxide KOH, methanol, and ethanol, procured from E. Merck Ltd., India, were used as initial precursors. Zinc acetate (0.5 M) was dissolved in 100 mL of methanol with continuous stirring for 2 h at room temperature (solution A). Simultaneously, 140 mmol KOH solution was prepared in 100 mL of methanol with refluxing through a water condenser with constant stirring for 2 h at 50 °C (solution B). Then solutions A and B were mixed with constant stirring for 2 h at 50 °C while refluxing. The final solution was allowed to cool at room temperature and aged overnight. This solution was centrifuged and washed several times with absolute ethanol and water to remove the impurities. The obtained white product was placed in a vacuum oven for 24 h at 50 °C to get white powders of ZnO.

A similar procedure was followed for the synthesis of Fe (20%)- and Co (20%)-doped ZnO nanoparticles. In this case, solution A consisted of a mixture of zinc and iron acetates for Fe doping and cobalt acetate for Co-doped samples. The rest of the method was same as above.

For the synthesis of a $ZnO@SiO_2$ matrix, some amount of ZnO was redispersed in ethanol, and simultaneously, the SiO_2 matrix was prepared by vigorously mixing 10 mL of tetraethylorthosilicate in 10 mL of ethanol and 5 mL of H_2SO_4 at 30 °C for 2 h. The resulting transparent solution and the ethanolic suspension of ZnO were mixed slowly with constant stirring at 30 °C. The Si/Zn solution ratio was kept at 30:1. After 2 h of constant stirring at 30 °C, the solution turned into a transparent, light yellow gel. This transparent, light yellow gel was further subjected to ultrasonication for another 2 h. The resulting gel-like mixture was kept in air for a few hours to give a thick gel, which was further dried and annealed at 500 °C in air, giving the final product. The details of $ZnO@SiO_2$ synthesis and characterizations results were reported elsewhere.[12]

2.2. Characterizations Used. The crystal structure, size, and shape of prepared ZnO nanoparticles were investigated using XRD and TEM. XRD was performed on a Rigaku D/max-2200 PC diffractometer operated at 40 kV/20 mA using Cu $K\alpha_1$ radiation with a wavelength of 1.54 Å in a wide-angle region from 25° to 70° on a 2θ scale. The size and morphology of the prepared nanophosphors were recorded by a transmission electron microscope, model Tecnai 30 G^2 S-Twin, operated at 300 kV accelerating voltage. In addition, a Reinshaw RM 2000 micro-Raman was employed to investigate the presence of defect states. The effects of the interaction of the ZnO nanoparticles with the *E. coli* cells were observed with a scanning electron microscope, model Quanta 200 MK2, operated at 25 kV in environmental scanning electron microscopy (ESEM) mode on the ZnO-treated *E. coli* films.

2.3. Toxicological Tests. Toxicological tests were performed on solid agar plates and also in liquid media with different concentrations of ZnO ranging from 0 μg/mL to 4096 μg/mL. The tubes and plates with ZnO nanoparticles were inoculated with bacterial cells and incubated at 37 °C for 18−20 h. The percentage of innoculum taken was (0.1%) of the growth medium. The inoculated cells were estimated to 200 CFU (colony forming units) per plate. Negative and positive control tubes contained only inoculated broth and free ZnO solution, respectively. The visual turbidity of the tubes was noted before and after incubation. After incubation, 30 μL of solution was taken from those tubes that appeared to have little or no cell growth and plated on nutrient agar plates to distinguish between the bacteriostatic and bactericidal properties of these nanoparticles. The plates were then incubated at 37 °C for 12−18 h, and the colonies were quantified. The MIC and MBC were thus evaluated from the above experiments.

For investigation of growth in dark, the Petri plates were wrapped with black paper to mimic dark conditions and incubated at 37 °C. Innoculation was performed in a dark room without any source of light, allowing a minimum amount of light exposure. Bacteriostatic properties were further supported by growth curve analysis. The optical density (OD) was recorded at 600 nm, which was chosen for OD measurement because it gives the actual absorbance; the absorbance of the cellular components does not lie in this wavelength range. Hence, this absorbance is totally in accordance with the change in turbidity, hence, the cell number. Positive controls (nanoparticles in LB medium, without inoculum) and negative control (LB medium with inoculum, without nanoparticles) were used to perform this measurement. A series of nanoparticle concentrations were taken to obtain the growth curves. The optical density of the negative control indicates the *E. coli* growth profile in the absence of nanoparticles, whereas to obtain the growth profile of *E. coli* cells in the presence of nanoparticles, the absorbance value of the positive controls at 600 nm were subtracted from the experimental values (LB medium containing inoculum and nanoparticles). For studying the growth curves in dark conditions, the entire conical flasks were covered with black paper, leaving the plug region. Exposure to light was mitigated as much as possible during performance of the tests.

The determination of qualitative antibacterial properties of these particles was also carried out by disk diffusion tests. This is a very cost-effective and quick method to confirm the susceptibility of bacterial cells to an antimicrobial agent and is useful for assessing the degree of antimicrobial properties if combined with other characterization methods. Antimicrobial agents (i.e., ZnO nanoparticles in the present case) were prepared in deionized sterile water to obtain stock solutions of the nanoparticles of 10 and 100 mg/mL. The agar plates were inoculated by confluent swabbing of bacterial suspension on the surface with the adjusted inoculum suspensions and allowed to dry for some time. Simultaneously, the antimicrobial agents (i.e., ZnO nanoparticles suspensions) were prepared in deionized sterile water to obtain stock solutions of the nanoparticles of 10 mg/mL and 100 mg/mL. Filter paper discs of 1 cm diameter were saturated with an aseptic suspension of ZnO stock solutions of optimized concentrations. The paper disks impregnated with the ZnO were aseptically placed onto the dried surface of the inoculated agar plate using ethanol and flame sterilized forceps. A ZnO-free filter paper disk was used as a control on solid agar plates. The plates were incubated at 37 °C under microaerophilic conditions. The antimicrobial agents diffuse from the carrier (disks) into the medium, producing a concentration gradient. Bacterial growth in the vicinity of the carrier occurs only when the concentration diffusing from the carrier is no longer sufficient to inhibit bacterial replication or when the bacterial cell is resistant to the antimicrobial agent. If the concentrations are sufficient to achieve inhibition, a circular region of no bacterial growth develops. This is called the zone of inhibition. After 24 h of incubation, clear distinct zones of inhibition were

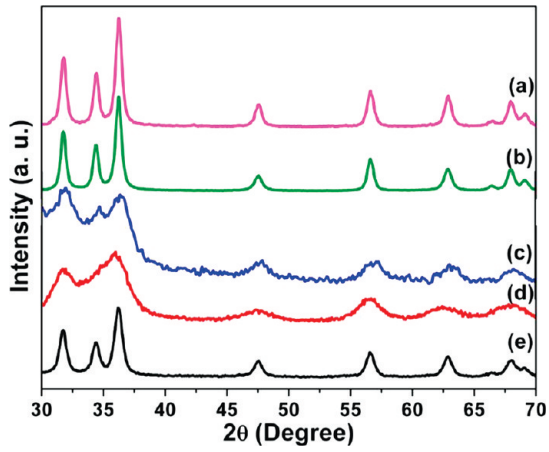

Figure 1. XRD spectra of the synthesized ZnO nanoparticles: (a) ZnO (200−300 nm), (b) ZnO (25 nm), (c) ZnO@SiO_2 (25 nm), (d) ZnO:Fe^{2+} (25 nm), and (e) ZnO:Co^{2+} (25 nm).

observed. These were then measured to estimate the differential qualitative growth.

3. Results and Discussion

Figure 1 represents (a) the XRD pattern of commercial ZnO (∼200−300 nm), (b) the XRD pattern of ZnO nanoparticles (∼25 nm), (c) the XRD pattern of ZnO@SiO_2 nanoparticles (∼25 nm), (d) the XRD pattern of ZnO:Fe^{2+} nanoparticles(∼25 nm), and (e) the XRD pattern of ZnO:Co^{2+} nanoparticles (∼25 nm). All the samples show broad peaks at the positions of 31.63°, 34.50°, 36.25°, 47.50°, 56.60°, 62.80°, 66.36°, 67.92°, and 68.91°, which are in good agreement with the standard JCPDS file for ZnO (JCPDS 36-1451, $a = b = 3.249$ Å, $c = 5.206$ Å) and can be indexed as the hexagonal wurtzite structure of ZnO having space group $P6_{3mc}$. The crystallite size, d, of these ZnO nanoparticles was estimated by Debye−Scherrer's equation and found to be nearly 25 nm for b, c, d, and e, whereas the commercial ZnO nanoparticles (i.e., a) shows crystallite size ∼200 nm. These results are in good agreement with the observed TEM results. In ZnO:Fe^{2+} and ZnO:Co^{2+} nanoparticles, at least up to the detection level of the XRD, no evidence of metal oxide or metal cluster was observed in XRD observations, suggesting almost total incorporation of Fe^{2+} or Co^{2+} to the Zn site in the host ZnO lattice, whereas in ZnO@SiO_2, a high background scattering was observed in the XRD pattern, suggesting the presence of a SiO_2 matrix, which was further confirmed by TEM and Raman investigations. Figure 2 shows the size and shape of the different samples. TEM images clearly show spherical particles having sizes ∼25 nm for b, c, d, and e. A very narrow size distribution of ZnO nanoparticles of 25 nm diameter was obtained with the addition of silica (Figure 2c); in Figure 2a, the particle size is ∼200 nm.

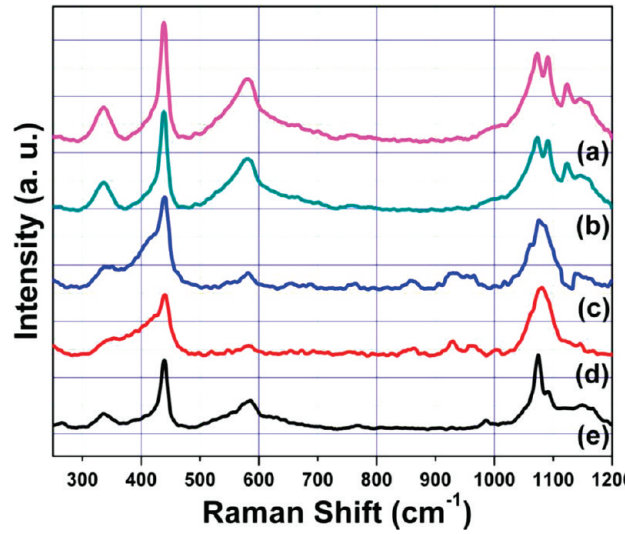

Figure 3. Raman spectra of the synthesized ZnO nanoparticles: (a) ZnO (200−300 nm), (b) ZnO (25 nm), (c) ZnO@SiO_2 (25 nm), (d) ZnO:Fe^{2+} (25 nm), and (e) ZnO:Co^{2+} (25 nm) nanoparticles.

Raman spectroscopic studies were carried out to understand the effects of defects on the microscopic structures of these nanoparticles and are shown in Figure 3. Several literature sources show that in hexagonal wurtzite ZnO, the following fundamental optical bands should exist, according to the group theory: E_2 (low) at 101 cm^{-1}, E_2 (high) at 437 cm^{-1}, A_1 (TO) at 380 cm^{-1}, A_1 (LO) at 574 cm^{-1}, E_1 (TO) at 407 cm^{-1}, and E_1 (LO) at 583 cm^{-1}. The low-frequency E_2 mode is associated with the vibration of a heavy Zn sublattice, and the high-frequency E_2 mode involves only the oxygen atoms. Raman spectra (Figure 3) showed a strong Raman shift signal at ∼437 cm^{-1}, which is due to the E_2 (high) mode of ZnO nanoparticles. These results were consistent with already reported works.[13−16]

The second-order vibrations were at 208, 334, and 1050−1200 cm^{-1}, whereas in ZnO:Co^{2+} nanoparticles (Figure 3e), Raman modes similar to those of ZnO as discussed above were observed. On the other hand, for ZnO@SiO_2 and ZnO/Fe nanoparticles (see Figure 3c, d), the presence of small peaks at ∼583 and 378 cm^{-1} were due to E_1 (LO) and A_1 (TO) modes of ZnO, respectively, and further confirmed that the oxygen vacancy is quite low in these samples. The sharpest and strongest peak at about 437 cm^{-1} is the strongest Raman mode in the wurtzite crystal structure. It is well-known that lattice defects and disorder could usually be introduced by exotic ion doping; defect-induced Raman modes would usually appear in defective crystals because the Raman selection rules are relaxed.[17] The other peaks appearing in the low-frequency region correspond to the second-order vibrational modes of ZnO. These results, along with XRD, further confirm that the ZnO nanoparticles are of hexagonal wurtzite structure without any impurity phase.

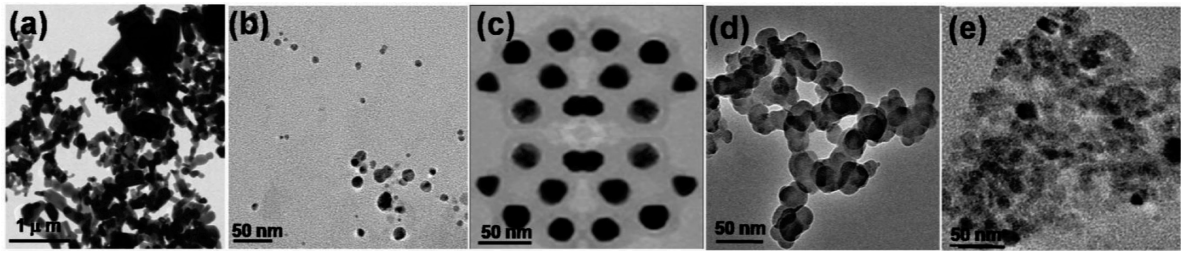

Figure 2. TEM images of (a) ZnO (200−300 nm), (b) ZnO (25 nm), (c) ZnO@SiO_2 (25 nm), (d) nanoparticles ZnO:Fe^{2+}, and (e) ZnO:Co^{2+} (25 nm) nanoparticles.

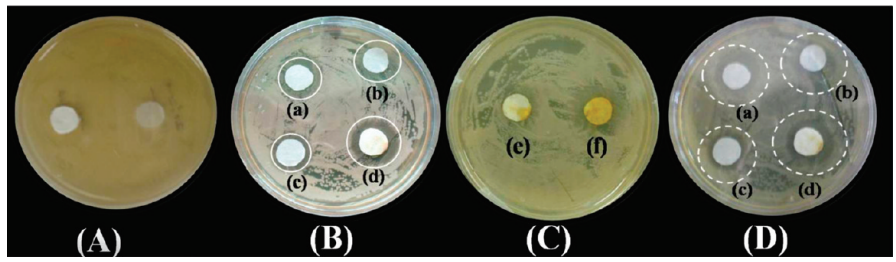

Figure 4. (A) Control plates with filter paper disks without any nanoparticles. (B) Disk diffusion tests with 10 mg/mL of (a) ZnO (200−300 nm), (b) ZnO (25 nm), (c) ZnO@SiO_2 (25 nm), and (d) ZnO:Co^{2+} (25 nm) nanoparticles. (C) Disk diffusion tests with 10 mg/mL of ZnO:Fe^{2+} (25 nm) (e) and 100 mg/mL ZnO:Fe^{2+} (25 nm) nanoparticles (f). (D) Image of disk B photographed after 4 months.

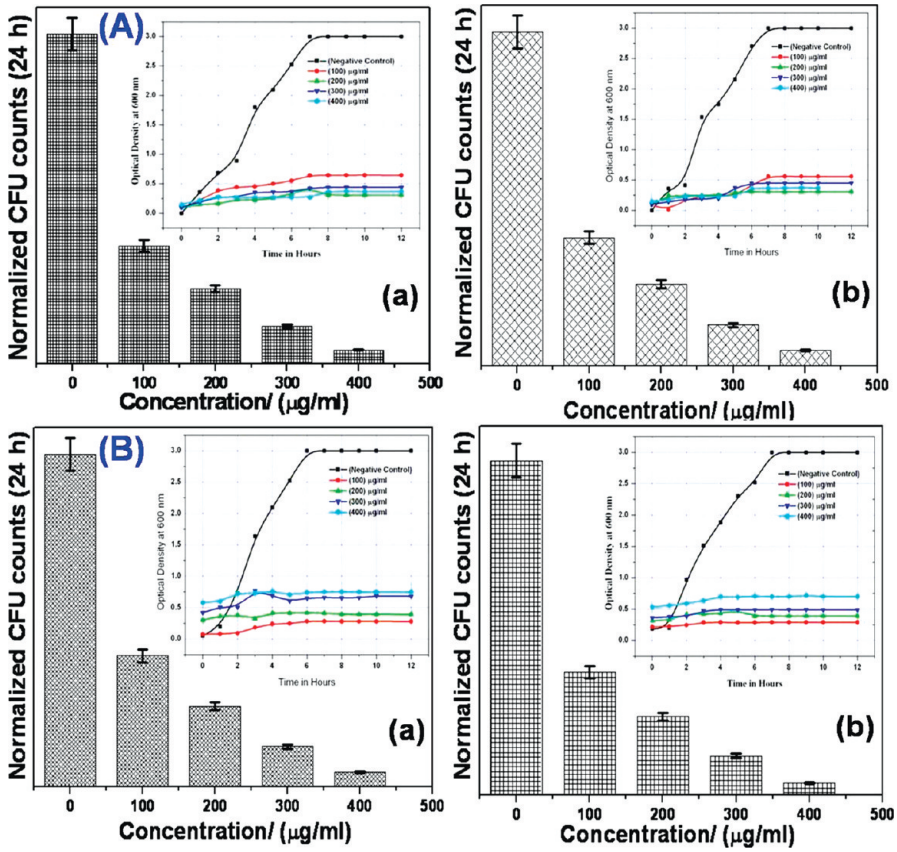

Figure 5. (A) Growth curves of bacterial cells treated with nanoparticles of size 25 nm under (a) dark and (b) light conditions. (B) Growth curves of bacterial cells treated with ZnO nanoparticles of size 200−300 nm under (a) dark and (b) light conditions.

Our results show that there was a significant change in the bactericidal property at different concentrations of ZnO nanoparticles and with changing properties of ZnO nanoparticles. The standard broth dilution tests were carried out at nanoparticle concentrations between 0 and 4096 μg/mL of the ZnO. MIC for ZnO (200−300 nm) nanoparticles was estimated to be 256−512 μg/mL. For ZnO (25 nm), the MIC lies between 128 and 256 μg/mL; for MBC, at >512 μg/mL in light and between 256 and 512 μg/mL under dark conditions. In comparison, Padmavathy et al.[18] reported the MIC between 0.8 and 8000 μg/mL for different concentrations of ZnO nanoparticles against the Gram negative bacterium *E. coli*. In our case, for Co^{2+}-doped ZnO, the determined MIC was 64−128 μg/mL, and the MBC was 128−256 μg/mL. On the other hand, for Fe-doped ZnO, there was no inhibition up to 2048 μg/mL. Results showed no bacteriocidal activity up to 4096 μg/mL and is only bacteriostatic at higher concentrations; that is, at >2048 μg/mL under light. For the bacterial samples treated with ZnO@SiO_2, the MIC lies between 1024 and 2048 μg/mL.

Figure 4A shows the disk diffusion tests that were performed on solid agar plates. Clear zones of inhibition were observed inside an open circle around the filter paper with distinct variations in the susceptibility of bacteria toward ZnO. Here, we can see that the zone of inhibition is at a maximum around the ZnO:Co^{2+} (25 nm)-treated filter paper and at a minimum around the ZnO@SiO_2- and ZnO:Fe^{2+}-treated filter paper, indicating that the ZnO nanoparticles with different modifications could differentially restrain the proliferation of *E. coli* cells. This shows the differences in susceptibility of the bacterial cells with the differences in functional properties The zones of inhibition measured were 25 mm for ZnO:Co^{2+} (25 nm), 21 mm for ZnO (25 nm), 19 mm for ZnO (200−300 nm), 17 mm for ZnO@SiO_2, and 8 mm for ZnO:Fe^{2+}. Figure 4D shows the same plate as in the case of Figure 4B when photographed after 4 months. It is clear from the Figure that the bacteria have grown well around most of the filter paper disk impregnated with nanoparticles except ZnO:Co^{2+} and ZnO@SiO_2, giving some

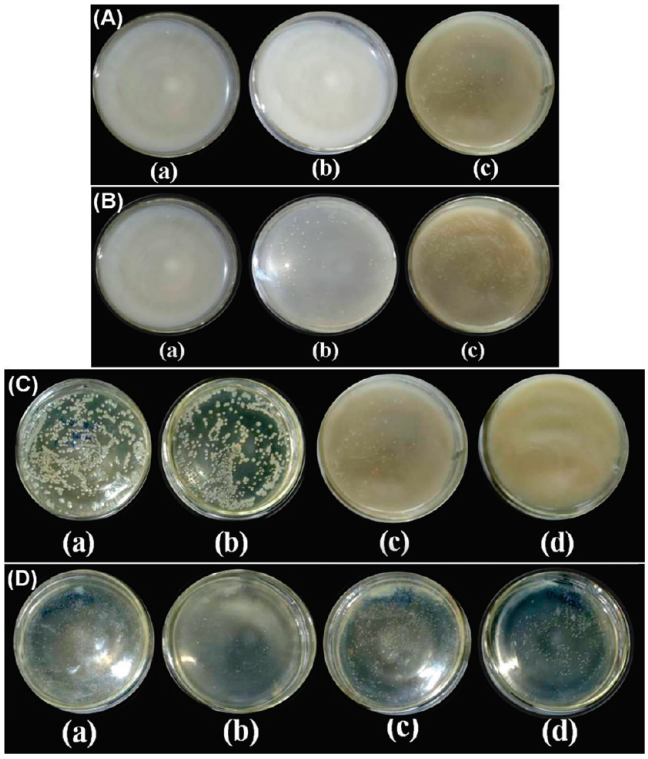

Figure 6. (A) Bacteria inoculated on plates with 4096 μg/mL of (a) ZnO:Co^{2+} (25 nm), (b) ZnO@SiO_2 (25 nm), and (c) ZnO:Fe^{2+} (25 nm) nanoparticles. (B) Bacteria inoculated on plates with 2048 μg/mL of (a) ZnO:Co^{2+} (25 nm), (b) ZnO@SiO_2 (25 nm), and (c) ZnO:Fe^{2+} (25 nm). (C) Colonies formed on control plates (without nanoparticles) under (a) dark and (b) light conditions; plates with 4096 μg/mL of ZnO:Fe^{2+} (25 nm) nanoparticles under (c) dark and (d) light conditions. (D) Colonies formed on plates treated with 128 μg/mL of ZnO:Co^{2+} (25 nm) nanoparticles under (a) dark and (b) light conditions; colonies formed on plates treated with 128 μg/mL of ZnO@SiO_2 (25 nm) nanoparticles under (c) dark and (d) light conditions.

indication that the bacteria may not have developed resistance toward these nanoparticles, unlike the other forms of ZnO.

Figure 5A shows growth curves of (a) bacterial cells treated with 25 nm nanoparticles under dark conditions and (b) bacterial cells treated with 25 nm nanoparticles under light. It can be seen that under dark conditions, the log phases are seen at lower ZnO concentrations, whereas under light, there is a significant delay in the log phase attainment, which is indicative of the fact that light has inhibited the growth of bacterial cells, but in the control there is no such delay. This throws light onto the fact that it is due to the presence of the nanoparticles in light that is inhibitory. Figure 5B shows growth curves of (a) bacterial cells treated with nanoparticles of size 200−300 nm under dark conditions and (b) bacterial cells treated with nanoparticles of size 200−300 nm under light. It is evident that the attainment of the stationary phase is early in all the cases under light, and the only log phase seen is in the case of the lowest concentration under dark conditions. In the case of 25 nm particles, the growth seems to occur at lower concentrations, and there is hardly any log phase seen at concentrations above 200 μg/mL. This seems to suggest that in the case of 25 nm sized particles, the growth occurs at a lower concentration, and no growth in the case of bacterial cells treated with larger particles.

Figure 6A shows bacteria inoculated on plates with (a) 4096 μg/mL of ZnO:Co^{2+} (25 nm), (b) 4096 μg/mL of ZnO@SiO_2 (25 nm), and (c) 4096 μg/mL of ZnO:Fe^{2+} (25 nm) nanoparticles. Figure 6B shows bacteria inoculated on plates with (a) 2048 μg/mL of ZnO:Co^{2+} (25 nm), (b) 2048 μg/mL of ZnO@SiO_2 (25 nm), and (c) 2048 μg/mL of ZnO:Fe^{2+} (25 nm) nanoparticles. Figure 6C show colonies formed on (a) control plates (without nanoparticles) under dark conditions, (b) control plates (without nanoparticles) in light, (c) plates with 4096 μg/mL of ZnO:Fe^{2+} (25 nm) nanoparticles under dark conditions, and (d) plates with 4096 μg/mL of ZnO:Fe^{2+} (25 nm) nanoparticles in light. Figure 6D shows colonies formed on (a) a plate with 128 μg/mL of ZnO:Co^{2+} (25 nm) nanoparticles under dark conditions, (b) a plate with ZnO:Co^{2+} (25 nm) nanoparticles in light, (c) a plate with 128 μg/mL of ZnO@SiO_2 (25 nm) nanoparticles in the dark, and (d) a plate with 128 μg/mL of ZnO@SiO_2 (25 nm) nanoparticles in light.

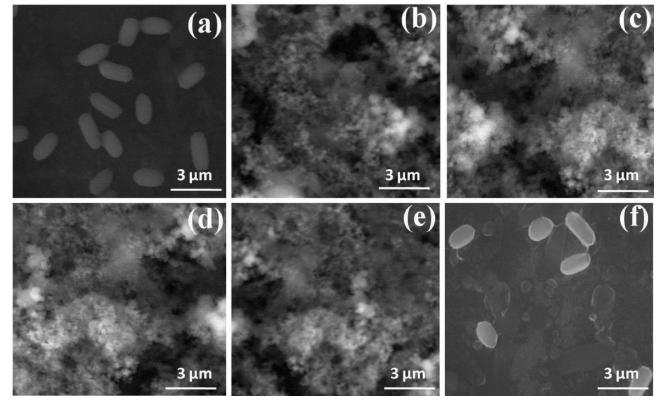

Figure 7. ESEM micrograph of *E. coli* cells treated with: (a) no nanoparticles (negative control), (b) 2048 μg/mL of ZnO (200−300 nm), (c) 2048 μg/mL of ZnO (25 nm), (d) 2048 μg/mL of ZnO:Co^{2+} (25 nm), (e) 2048 μg/mL of ZnO@SiO_2 (25 nm), and (f) 2048 μg/mL ZnO:Fe^{2+} (25 nm) nanoparticles.

For the plates, the concentration of ZnO nanoparticles was varied between 0 and 4096 μg/mL. The presence of these ZnO nanoparticles at concentrations of >512 μg/mL caused more than 98% inhibition of bacterial growth. A concentration between 64 and 512 μg/mL could inhibit bacterial growth by 30−50%. For concentrations between 16 and 64 μg/mL, only a slight decrease in the number of bacterial colonies was detected. In case of ZnO@SiO_2 and ZnO:Fe^{2+}, concentrations >2048 are inhibitory, and lower concentrations do not seem to affect bacterial growth. ZnO:Co^{2+}-treated bacterial cells showed inhibition between 128 and 256 μg/mL; ZnO:Co^{2+} treated cells showed inhibition at 256 μg/mL under dark conditions. Inhibition in light was greater when compared to the dark in all cases. These results indicate that the differences in toxicity behavior are with concentrations and with the varying properties of the ZnO nanoparticles. The differences in growth under light and dark conditions have been demonstrated and are quite distinct.

Figure 7 shows the representative ESEM micrograph of *E. coli* cells treated with (a) no nanoparticles (negative control) showing intact *E. coli* cells, (b) 2048 μg/mL of ZnO (200−300 nm), (c) 2048 μg/mL of ZnO (25 nm), (d) 2048 μg/mL of ZnO:Co^{2+} (25 nm), (e) 2048 μg/mL of ZnO@SiO_2 (25 nm), and (f) 2048 μg/mL ZnO:Fe^{2+} (25 nm) nanoparticles, showing reduction in cell number, but not complete bacteriostatic activity. While panels b, c, and d show complete bacteriostatic activity. These results are in agreement with the growth curve and CFU count results showing a very gradual decrease in cell numbers with an increase in nanoparticle concentration.

The most important factors that seem to play a major role in governing the toxicity mechanism could be attributed to the differences in oxygen vacancies with the changing properties of ZnO nanoparticles, as is evident from the Raman spectra in Figure 3. The antibacterial activity of the small-sized particles

TABLE 1: The Comparative Results of CFU Counts

concn, μg/mL	nanoparticles									
	ZnO (200−300 nm)		ZnO (20−30 nm)		ZnO@SiO_2		ZnO:Co^{2+}		ZnO:Fe^{2+}	
	light	dark	light	dark	light	dark	light	dark	light	dark
0	++++	++++	++++	++++	++++	++++	++++	++++	++++	++++
8	++++	++++	++++	++++	++++	++++	++++	++++	++++	++++
16	++++	++++	++++	++++	++++	++++	+++	+++	++++	++++
32	++++	++++	++++	++++	++++	++++	++	+++	++++	++++
64	+++	+++	+++	++++	++++	+++	−	+	++++	++++
128	++	++	++	+++	++	++	−	−	+++	++++
256	+	+	−	+	+	+	−	−	+++	+++
512	−	+	−	−	+	+	−	−	++	++
1024	−	−	−	−	+	+	−	−	+	+
2048	−	−	−	−	−	+	−	−	+	+

may be due to the increase in the surface-to-volume ratio of the particles and, hence, a greater penetrating ability. In the case of ZnO (25−30 nm) nanoparticles' surface area being greater, the reactivity is more like we know from the properties of particles in the nanoregime. The increase in oxygen vacancies renders the particles to be positively charged and, hence, increases the electrostatic interactions between the positively charged particles and the negative cell wall surface.

For cells treated with ZnO@SiO_2, the reduction in toxicity may be because SiO_2 provides good coverage of the ZnO surface and acts as an energetic barrier, preventing the escape of photogenerated carriers to outside the confined ZnO nanoparticles. Surface modifications with SiO_2 help in surface passivation, reducing the oxygen defect and, hence, reducing the toxicity of the particles. In the case of ZnO@SiO_2, the holes were confined within the ZnO, and the electrons were delocalized over the entire embedded matrix. The doping of ZnO nanoparticles by Fe^{2+} or Co^{2+} replaces the Zn^{2+} with cations such as Fe^{2+} or Co^{2+}; hence, even though the overall positive charge may not have been disturbed, the Zn^{2+} ions in the lattice structure of the ZnO nanoparticles have been modified by the Fe^{2+} or Co^{2+} ions.

In the case of ZnO:Fe^{2+} the mitigation in toxicity may be due to Fe^{2+}'s doping in the host lattice of ZnO. This is further supported by the fact that, in the Raman spectra, plate e has a high intensity peak at 590, when compared to plates c and d, meaning that e has greater oxygen vacancies and seems to cause maximum toxicity. Several explanations have been given to explain the mechanism by which ZnO causes toxicity to cells. Preliminary results of cellular internalization of ZnO nanoparticles and cell wall disorganization have been shown by Brayner et al.[19] Brayner et al. showed *E. coli* cells being damaged morphologically at lower ZnO concentrations and cell rupture at higher concentrations due to internalization of ZnO nanoparticles. The valence band holes created by the photocatalytic effect of ZnO nanoparticles in the presence of light cause the formation of hydroxide and superoxide molecules, which are antimicrobial agents. Several other studies[20] have reported the cytotoxicity of ZnO, DNA damage, and oxidative lesions determined using the comet assay. ZnO showed effects on cell viability as well as DNA damage,[21] whereas smaller size ZnO has a higher antibacterial activity.[18]

4. Conclusions

These results indicate that toxicity varies with the structural and chemical properties and can be modulated for use as a bactericidal agent. Our experimental results revealed that size, oxygen defects in ZnO, the presence of activator atoms in the host lattice, and surface modifications, etc. play a critical role in the toxicological behavior of nanoparticles. Growth kinetics studies show that ZnO nanoparticles interfere with the bacterial cell growth as the cells proceed from lag phase to stationary phase, as is evident from growth curve analysis. ZnO in SiO_2 matrix and Fe^{2+}-doped ZnO showed a reduction in the toxic effects of these nanoparticles and doping with Co^{2+} increases the antibacterial activity as compared with ZnO nanoparticles. The antibacterial mechanism is enhanced in the presence of light in all the above cases. Overall, the antibacterial behavior increased from Fe^{2+}-doped ZnO to ZnO@SiO_2 to ZnO (200−300 nm) to Co^{2+}-doped ZnO to ZnO (25−30 nm). Modifications in ZnO can be performed to reduce the toxicity and render them applicable for biomedical applications. The applications of ZnO for various purposes can be preformed with suitable doping and capping agents. Still, further studies pertaining to their effects on eukaryotic cells have to be done before technological applications of ZnO nanoparticles.

Acknowledgment. The authors are thankful to DST and CSIR, India, for supporting Nanotechnology Application Centre under IRHPA, Nano-Mission, and NMITLI schemes.

References and Notes

(1) Jiang, P.; Zhou, J. J.; Fang, H. F.; Wang, C. Y.; Wang, Z. L.; Xie, S. S. *Adv. Funct. Mater.* **2007**, *17*, 1303.
(2) Zhou, J.; Xu, N. S.; Wang, Z. L. *Adv. Mater.* **2006**, *18*, 2432.
(3) Ito, M. *Biomaterials* **1991**, *12*, 41.
(4) Ørstavik, D.; Hongslo, J. K. *Biomaterials* **1985**, *2*, 129.
(5) Yamamoto, O.; Komatsu, M.; Sawai, J.; Nakagawa, Z. *J. Mater. Sci. Mater. Med.* **2008**, *19*, 1407.
(6) Reddy, K. M. *Appl. Phys. Lett.* **2006**, *90*, 13902.
(7) Adams, L. K.; Lyon, D. Y.; Alvarez, P. J. J. *Water Res.* **2006**, *40*, 3527.
(8) Wang, X.; Yang, F.; Yang, W.; Yang, X. *Chem. Commun.* **2007**, *42*, 4419.
(9) Applerot, B. G.; Lipovsk, A.; Dror, R.; Perkas, N.; Nitzan, Y.; Lubart, R.; Gedanken, A. *Adv. Funct. Mater.* **2009**, *19*, 842.
(10) Yamamoto, O.; Komatsu, M.; Sawai, J.; Nakagawa, Z. *J. Mater. Sci.: Mater. Med.* **2004**, *15*, 847.
(11) Lipovsky, A.; Tzitrinovich, Z.; Friedmann, H.; Applerot, G.; Gedanken, A.; Lubart, R. *J. Phys. Chem. C* **2009**, *113*, 15997.
(12) Sharma, P. K.; Dutta, R. K.; Kumar, M.; Singh, P. K.; Pandey, A. C. *J. Lumin.* **2009**, *129*, 605.
(13) Wang, Z.; Zhang, H.; Zhang, L.; Yang, J.; Yan, S.; Wang, C. *Nanotechnology* **2003**, *14*, 11.
(14) Damen, C.; Porto, S. P. S.; Tell, B. *Phys. Rev.* **1996**, *142*, 570.
(15) Zhang, Z.; Huang, B.; Yu, Y.; Guo, D. *Mater. Sci. Eng. B* **2001**, *86*, 109.
(16) Koyano, M.; Quoc Bao, P.; ThanhBinh, L. T.; Hong, H. L.; Ngoc Long, N.; Katayama, S. I. *Phys. Status Solidi A* **2002**, *193*, 125.
(17) Chartier, P. D.; Arco, R.; Dovesi, V.; Saunders, R. *Phys. Rev. B* **1999**, *60*, 14042.
(18) Padmavathy, N.; Vijayaraghavan, R. *Sci. Technol. Adv. Mater.* **2008**, *9*, 035004.
(19) Brayner, R.; Ferrari-Iliou, R.; Brivois, N.; Djediat Benedetti M, F.; Fiévet, F. *Nano Lett.* **2006**, *6* (4), 866.
(20) Gojova, A.; Guo, B.; Kota, R. S.; Rutledge, J. C.; Kennedy, I. M.; Barakat, A. I. *Environ. Health Perspect.* **2007**, *115*, 403.
(21) Karlsson, H. L.; Cronholm, P.; Gustafsson, J.; Moller, L. *Toxicol. Lett.* **2009**, *188*, 112.

JP1004488